On the attenuation of the dynamic yield point of shocked aluminum using elastodynamic simulations of dislocation dynamics

Beñat Gurrutxaga–Lerma, Daniel S Balint, and Daniele Dini
Department of Mechanical Engineering
Imperial College London, London SW7 2AZ, UK

Daniel E Eakins and Adrian P Sutton
Department of Physics
Imperial College London, London SW7 2AZ, UK

When a metal is subjected to extremely rapid compression, a shock wave is launched that generates dislocations as it propagates. The shock wave evolves into a characteristic two-wave structure, with an elastic wave preceding a plastic front. It has been known for more than six decades that the amplitude of the elastic wave decays the further it travels into the metal: this is known as "the decay of the elastic precursor". The amplitude of the elastic precursor is a dynamic yield point because it marks the transition from elastic to plastic behaviour. In this letter we provide a full explanation of this attenuation using the first method of dislocation dynamics to treat the time dependence of the elastic fields of dislocations explicitly. We show that the decay of the elastic precursor is a result of the interference of the elastic shock wave with elastic waves emanating from dislocations nucleated in the shock front. Our simulations reproduce quantitatively recent experiments on the decay of the elastic precursor in aluminum, and its dependence on strain rate.

The dynamic behaviour of crystalline solids subjected to shock compression plays a central role in diverse applications, including bird strikes in aerospace [1], crashworthiness in the automobile industry [2], and manufacturing processes such as laser shock peening [3], amongst many others. Upon being shocked within a range of strain rates and pressures of typically $10^6 - 10^{10}\mathrm{s}^{-1}$ and $5 - 50\mathrm{GPa}$ [1], the shock front in crystalline materials often displays a characteristic two–wave structure near the loading surface: the *plastic* wave front leading to the *Hugoniot shocked state* is preceded by an *elastic* precursor wave [1]. The amplitude of the elastic precursor wave decays as the wave front advances[1, 4]—a phenomenon known as the 'decay of the elastic precursor'. The amplitude of the elastic wave marks the onset of plasticity, i.e. it is the dynamic yield point. The subsequent *plastic wave* is commonly ascribed to the generation and motion of dislocations, the agents of plasticity in crystalline solids[9].

The cause of its attenuation remains unclear after six decades [4–8]. Clifton and Markenscoff [4] calculated analytically the amplitude attenuation of a planar elastic shock wave caused by the destructive interference of elastic wavelets emanating from pre-existing dislocations set into motion by the passage of a shock wave of infinite strain rate; dislocation generation by the shock was neglected. Consequently, the elastic precursor decay was attributed to the density and initial velocity of pre-existing dislocations. Armstrong et al.[10] studied the dislocation relaxation mechanisms during high strain rate shock loading, concluding that dislocation *generation* dominates plastic relaxation under shock loading. This is because the number of pre-existing dislocations is about two to three orders of magnitude less than that generated during the shock[1, 4, 7].

In this letter we show that we can account for the experimentally observed residual dislocation densities created by shock loading by assuming no pre-existing dislocations and that dislocations are generated within and behind the shock front. We go on to offer a complete explanation of the attenuation of the dynamic yield point, employing our recently developed method of Dynamic Discrete Dislocation Plasticity (D3P) [11]. Modern computing resources enable the simulation of crystalline metals subjected to shock loading using molecular dynamics (MD) simulations[12–14], but these are unable to discriminate between the effects of dislocations and other mechanisms in plastic relaxation processes. In contrast to MD, discrete dislocation dynamics (DDD) methods [15–18] enable the simulation of much larger systems over longer timescales.However, conventional DDD methods are inappropriate for the study of high strain rate shock compression, because they neglect the time dependence of the fields of moving dislocations. We showed in [11] that at high strain rates this leads to violation of causality because dislocation sources may be activated ahead of the shock.

We compare our simulations with a series of shock compression experiments performed at room temperature on an equivalent length and time scale. In these experiments, a range of μm-scale aluminum films were subjected to shock loading using a spectrally shaped laser pulse (fig.1). The development of the two-wave structure was probed using a pair of off-axis displacement interferometers, with time resolution approaching several ps. By maintaining a constant drive energy and varying the film thickness, the yield point was observed to decay from 12GPa for 2μm to 4.3GPa after 8μm [19].

Our D3P model simulates a single crystal sample of FCC aluminum at room temperature depicted in fig.1, with Young's modulus $E = 63.2\mathrm{GPa}$, shear modulus $\mu = 28.3\mathrm{GPa}$, density $\rho = 2700\mathrm{kg/m}^3$, and Burgers vec-

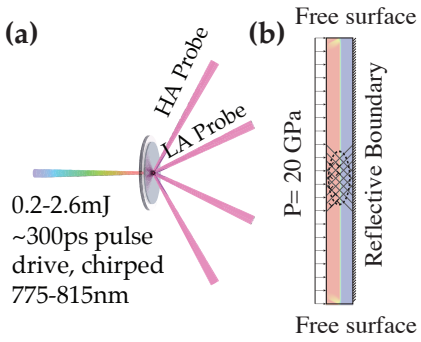

FIG. 1. Experimental set-up (a) and D3P simulation (b).

tor $b = \frac{a\sqrt{2}}{2} = 2.85\mathring{A}$. The sample is 10μm wide and 1μm thick. Following [20] we assume 3 slip planes at $\pm 54.7°, 0°$ to the shock front's normal. The sample is initially dislocation free, and loaded with an instantaneous 20GPa pressure on its left side. A reflective boundary condition is applied on the right side, whereas the top and bottom sides are left traction-free. Due to the loading, a shock front is generated and propagates through the material, triggering dislocation activity. The simulation finishes when the front reaches the reflective surface. The strain rate is enforced numerically (see *Supplementary Material*).

D3P tracks the time-dependent fields of injected and non-uniformly moving straight edge dislocations by solving the Navier-Lamé equation under plane strain conditions. Plane strain is a reasonable approximation here since a strongly uniaxial compressive shock load is applied over a relatively large area, orders of magnitude thinner in the direction of propagation. In D3P, the resulting elastic fields propagate at the two speeds of sound[11], which ensures causality is satisfied.

We assume the generation and motion of dislocations follows the constitutive rules of D3P [11]. The mobility law of dislocations is adjusted to account for the likely presence of high speed dislocations [1, 18, 21, 23–28]; data about the mobility of dislocations is extracted from MD simulations of aluminum [22] (see *Supplementary Materials*).

Two generation mechanisms are allowed: homogeneous nucleation and Frank–Read sources. At high strain rates Frank–Read sources are too slow with respect to the shock front's rise time to play a significant role in generating dislocations (see *Supplementary Material*). Thus, faster dislocation generation mechanisms must be considered. Smith[29], Hornbogen[30], Meyers and coworkers [31, 32], Shehadeh et al.[37] (using elastostatics) and Armstrong et al.[21] have all proposed dislocation generation processes involving homogeneous nucleation. Recent simulations show that the stress levels required to nucleate dislocations homogeneously are about the ideal shear lattice resistance ($\mu/18 - \mu/(4\pi)$), easily achievable in shock loading (vid.[33–35]). Recent

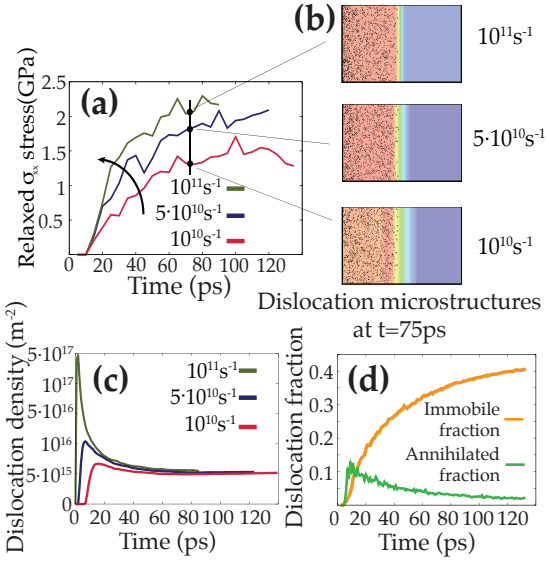

FIG. 2. (a) shows the accumulated relaxation effect of the dislocation fields at the shock front, for different strain rates. (b) shows the dislocation microstructures for different strain rates at $t = 75ps$, (c), shows the increase in ρ_{dis} with the strain rate. (d) shows the immobile and the annihilated fractions of dislocations for 10^{10}s^{-1}.

MD simulations[14, 36] also suggest that homogeneous nucleation is a primary source of dislocation loops, particularly for strain rates larger than 10^8-10^9s^{-1} [36]. Here homogeneous nucleation sources are assumed to operate instantaneously with activation stresses much higher that those for Frank-Read sources (see *Supplementary Material*).

We report a series of simulations in which the initial shock's amplitude was constant at 20GPa. These simulations concern the study of the elastic precursor and the early onset of the plastic wave. By varying the shock's width, three strain rates were imposed: 10^{10}s^{-1}, $5 \cdot 10^{10}\text{s}^{-1}$ and 10^{11}s^{-1}. These strain rates are close to those found by Crowhurst et al. [38] to lead to overdriven shocks. Fig.2 shows the σ_{xx} fields of dislocations, measured by averaging their elastodynamic stresses along a line parallel to the front and immediately behind it; its positive (tensile) magnitude interferes with the front's negative (compressive) amplitude. The elastic precursor decay is obtained by subtracting the corresponding curve shown in fig.2 from a reference hyper-elastic state. Fig.2 is consistent with experimental observation that the rate of decay increases with the strain rate [39]. Here the strain rate's effect is not entirely comparable to experiment, as in the latter the magnitude of the shock itself would vary too[40]. Nevertheless, fig.2 shows that an increase in the strain rate invariably leads to a higher relaxation of the shock; for the same time interval, a higher strain rate signifies that a larger area is subjected to higher stresses, resulting in a higher number of dislocations being generated within the front. As discussed below, there is a further significant contribution to the

relaxation from the velocity-dependence of the dislocations' elastic fields.

Fig.2 also shows the evolution of the dislocation density ($\rho_{\rm dis}$) for the three strain rates, calculated as the number of dislocations in the system at time t divided by the area swept by the front up to t. In fig.2 $\rho_{\rm dis}$ tends to saturate after an initial burst. The decay from this initial burst is a geometric effect: the number of dislocations tends to increase in proportion to the height of the sample, but the area behind the front increases in proportion to both the sample height and $c_l \cdot t$. Following this burst, dislocation dipoles are generated at a reduced steady rate which leads to the saturated $\rho_{\rm dis}$ seen in fig.2.

The computed $\rho_{\rm dis} \approx 6 \cdot 10^{15}{\rm m}^{-2}$ is of the same order of magnitude as that measured experimentally [1], and comparable to that predicted by analytical models such as that by Meyers et al.[32], which predicts a $\rho_{\rm dis} = 2.5{\cdot}10^{15}{\rm m}^{-2}$ for aluminum shocked at 20GPa. The dislocation structures at the front (see fig. 4), resemble those expected from the classical Smith-Hornbogen interface [21, 29, 30], with positive 'shielding' dislocations trailing just behind the front and negative 'anti-shielding' dislocations moving rapidly away from it. However, the nucleation process here is much more gradual, as it accounts for the strain rate of the shock front, and takes place not only at the front but behind it.

At these strain rates, Frank–Read sources have no effect on the elastic precursor decay. With $\approx$ 40ps activation times, they can generate only two or three dipoles throughout the simulation, and they are activated long after the front has passed; thus, the elastic fields of the newly generated dislocations cannot influence the front. We find the number of dislocations nucleated homogeneously is two orders of magnitude larger than those generated by Frank–Read sources. These results indicate that the relative contribution of each of these mechanisms of dislocation generation depends on the strain rate.

Fig.2 shows the evolution of the immobile fraction of dislocations, defined as those that move at speeds less than 100m/s. After 120ps this fraction increases to $40-45\%$. Thus, a significant fraction of the dislocations are effectively halted due to the sudden increase in $\rho_{\rm dis}$ in the wake of the front. Fig.2 also shows the number of annihilated dislocations. Most annihilations correspond to dipoles that are nucleated homogeneously with separations between the dislocations too small to overcome their mutual attraction. As the front proceeds it is seen that an increasing fraction of dislocations survives.

Fig.3 shows a comparison of the experimental data for aluminum at $10^{10}{\rm s}^{-1}$, and our simulated results up to 350ps at the same strain rate. To simulate the longer times the longitudinal sample size had to be increased from 1μm to 3.5μm while keeping the lateral dimension 10μm; the aspect ratio is enough to ensure that release waves do not reach the mid sections. The simulations were not extended further owisng to computational limitations associated with longer timescales. The decay with time of the elastic precursor can be fitted to

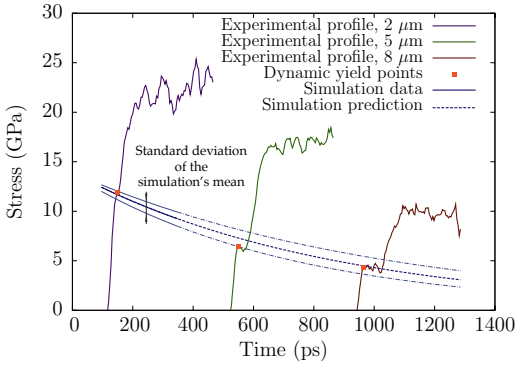

FIG. 3. Experimental vs simulated decay rate. The solid blue line is an exponential fit to our simulations; its extrapolation beyond 350ps is shown as a broken line. The broken lines on either side of this fit represent the standard deviation of the simulation's mean from the fit.

$f(t) = Ae^{-m\cdot t}$. The logarithmic decay rate is defined as $m = -\frac{1}{f}\frac{df}{dt}$. With a strain rate of $10^{10}{\rm s}^{-1}$ we obtain in our simulations $m = 0.0012 \pm 0.0002$. The experimental data for aluminum obtained by Whitley et al. [19] for a strain rate of $10^{10}{\rm s}^{-1}$ yields a logarithmic decay rate of $m = 0.001259$.

When a dipole is generated within the shock front, one dislocation of each dipole has a velocity component anti-parallel to shock front's velocity, and its stress wave is 'anti-shielding' [42] because it constructively interferes with the shock front's compressive amplitude. The other dislocation, with a velocity component parallel to the front's velocity, is a 'shielding' dislocation, as it destructively interferes with (decreases) the front's compressive amplitude. The cumulative effect of the shielding dislocations is greater than the effect of the anti-shielding dislocations, because the former are within the front for much longer. Thus, as first suggested by Clifton and Markenscoff [4], the cause of the elastic precursor decay is the cumulative and destructive interference of elastic waves emanating from shielding dislocations at the shock front. In this work dislocations are nucleated within the front, whilst in [4] they were pre-existing.

The destructive interference is greater at larger strain rates. Fig.4(a) shows a snapshot of the dislocation structure at the front at $t = 60ps$, together with their σ_{xx} fields, with $\dot{\epsilon} = 10^{10}{\rm s}^{-1}$. The dislocations in fig.4(a) are seen to organise themselves in structures reminiscent of a Smith-Hornbogen interface [21, 29, 30]; this results in a net plastic relaxation of the compressive elastic shock front. Fig.4(b), idealises the dislocation structure to a Smith–Hornbogen interface, with shielding dislocations moving frontwards, and anti-shielding dislocations moving away from the front (shown respectively in red an blue in fig.4(b)). Fig.4(c) shows the σ_{xx} fields of a single Smith–Hornbogen interface for two different dislocation speeds, 2000m/s and 3000m/s, assuming all dislocations move with the same speed. Because the shock front propagates with c_l, only the longitudinal wave component of

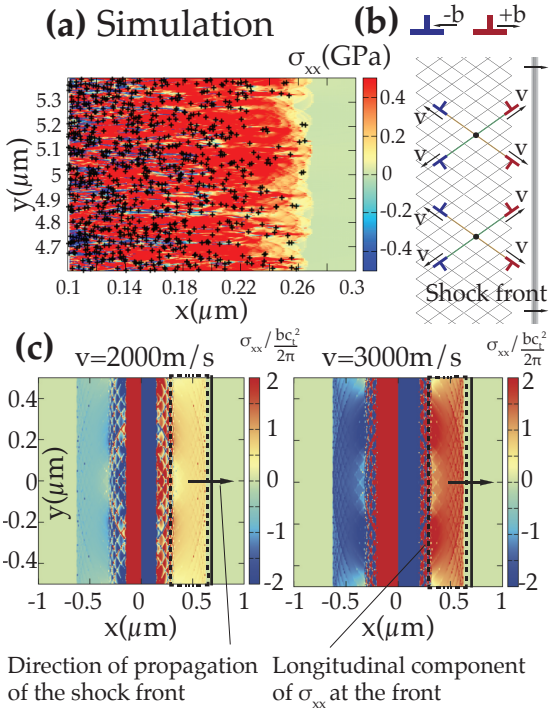

FIG. 4. (a) dislocation structure and its associated σ_{xx} field; (b) the dislocation structure is idealised by the Smith–Hornbogen interface. Red dislocations are shielding; blue are anti-shielding. (c) shows the σ_{xx} fields of the idealised dislocation configuration seen in (b).

each dislocation's field can keep up with the front and contribute to the plastic relaxation of the shock wave.

An analysis of the longitudinal component of the σ_{xx} field in fig.4(c) shows that its magnitude almost doubles when the dislocations' speed increases from $v_{\rm dis} = 2000$m/s to $v_{\rm dis} = 3000$m/s. This arises from the contraction of the dislocation fields in the direction of motion as $v_{\rm dis}$ increases. The contraction exists only ahead of the dislocation, in the direction of motion; behind the dislocation the magnitude of its fields tends to decrease. Consider the shielding dislocations: with increasing speed, the magnitude of the longitudinal component of σ_{xx} increases ahead of the dislocations, contributing to a greater relaxation of the shock front; this effect persists longer because the dislocations are moving faster towards the shock front. For anti-shielding dislocations, since they move away from the front, increasing their speed results in a relative decrease in the magnitude of the longitudinal component of σ_{xx} influencing the front. Because they move faster away from the front, they influence the shock front for less time. As a result, the amplitude of the shock wave is reduced much more by the shielding dislocations than it is increased by the anti-shielding dislocations, and this effect is magnified by increasing the strain rate.

We conclude that the dynamic yield stress is determined by an interference phenomenon between the elastic precursor wave and the elastic waves of shielding dislocations generated at the front. The increasing attenuation of the dynamic yield point with increasing strain rate (vid.fig.2), is a direct result of the elastodynamic fields of moving dislocations. This insight has been achieved by simulating the elastodynamic fields of dislocations nucleated and propagating as a result of the shock, a unique feature of D3P. Using D3P we have also explained the increasing attenuation of the dynamic yield stress with increasing strain rate within the shock.

Our results highlight the importance of dislocation generation mechanisms in relaxation processes at very high strain rates. Although at the strain rates probed here Frank–Read sources are generally too slow to be activated before the front is relaxed by homogeneously nucleated dislocations, it seems possible they may be involved in relaxation at much lower strain rates via the same mechanism. We believe that D3P simulations will provide further insights into plasticity at high strain rates, such as one finds in adiabatic shear, deformation twinning and martensitic transformations, and dynamic fracture.

ACKNOWLEDGMENTS

This work was funded by the EPSRC under grant no. EP/G036888/1. B.G.-L. acknowledges the support of the Department of Education of the Basque Government.

[1] M. Meyers, *Dynamic Behavior of Materials* (John Wiley, 1994).
[2] S. Hiermaier, *Structures under crash and impact* (Springer, 2007).
[3] C. Montross, T. Wei, L. Ye, G. Clark, and Y.-W. Mai, International Journal of Fatigue **24**, 1021 (2002).
[4] R. Clifton and X. Markenscoff, J. Mech. Phys. Solids **29**, 227 (1981).
[5] J. Campbell, Acta Metallurgica **1**, 706 (1953).
[6] J. Taylor, J. Appl. Phys. **36** (1965).
[7] Y. Partom, J. Appl. Phys. **59**, 2716 (1986).
[8] B.J. Demaske, V.V. Zhakhovsky, N.A. Inogamov, and I.I. Oleynik, Phys. Rev. B **87**, 054109 (2013).
[9] J. Hirth and J. Lothe, *Theory of Dislocations*, 2nd ed. (Krieger, 1991).
[10] R. Armstrong, W. Arnold, and F. Zerilli, J. Appl. Phys. **105**, 023511 (2009).
[11] B. Gurrutxaga-Lerma, D. Balint, D. Dini, D. Eakins, and A. Sutton, Proc. Roy. Soc. A **469**, 20130141 (2013).
[12] V. Bulatov, F. Abraham, L. Kubin, B. Devincre, and S. Yip, Nature **391**, 669 (1998).
[13] E. Bringa, A. Caro, Y. Wang, M. Victoria, J. McNaney,

B. Remington, R. Smith, B. Torralva, and H. Van Swygenhoven, Science **309**, 1838 (2005).
[14] E. Bringa, K. Rosolankova, R. Rudd, B. Remington, J. Wark, M. Duchaineau, D. Kalantar, J. Hawreliak, and J. Belak, Nature Materials **5**, 805 (2006).
[15] E. Van der Giessen and A. Needleman, Modelling Simul. Mater. Sci. Eng. **3**, 689 (1995).
[16] L. Kubin and G. Canova, Scripta Metallurgica **27**, 957 (1992).
[17] V. Bulatov and W. Cai, *Computer simulations of dislocation* (Oxford Univ. Press, Oxford, UK, 2006).
[18] M. Shehadeh, H. Zbib, and T. Diaz de la Rubia, Int. J. Plasticity **21**, 2369 (2005).
[19] V. Whitley, S. McGrane, D. Eakins, C. Bolme, D. Moore, and J. Bingert, J. Appl. Phys. **109**, 013505 (2011).
[20] J. Rice, Mechanics of Materials **6**, 317 (1987).
[21] R. Armstrong, W. Arnold, and F. Zerilli, Metallurgical and Materials Transactions A **38**, 2605 (2007).
[22] D. Olmsted, L. Hector, W. Curtin, and R. Clifton, Modelling Simul. Mater. Sci. Eng. **13**, 371 (2005).
[23] J. Hirth, H. Zbib, and J. Lothe, Modelling Simul. Mater. Sci. Eng. **6**, 165 (1998).
[24] L. Pillon, C. Denoual, and Y.P. Pellegrini, Phys. Rev. B **76**, 224105 (2007).
[25] Y.P. Pellegrini, Phys. Rev. B **90**, 054120 (2014).
[26] R. Beltz, T. Davis, and K. Malén, physica status solidi (b) **26**, 621 (1968).
[27] P. Gillis and J. Kratochvil, Philosophical Magazine **21**, 425 (1970).
[28] H. Zbib and T. Diaz de la Rubia, Int. J. Plasticity **18**, 1133 (2002).
[29] C. Smith, Trans. Met. Soc. AIME **212**, 574 (1958).
[30] E. Hornbogen, Acta Metallurgica **10**, 978 (1962).
[31] M. Meyers, Scripta Metallurgica **12**, 21 (1978).
[32] M. Meyers, F. Gregori, B. Kad, M. Schneider, D. Kalantar, B. Remington, G. Ravichandran, T. Boehly, and J. Wark, Acta Materialia **51**, 1211 (2003).
[33] M. Tschopp and D. McDowell, J. Mech. Phys. Solids **56**, 1806 (2008).
[34] M. Gutkin and I. Ovidko, Acta Materialia **56**, 1642 (2008).
[35] S. Aubry, K. Kang, S. Ryu, and W. Cai, Scripta Materialia **64**, 1043 (2011).
[36] B. Holian and P. Lomdahl, Science **280**, 2349 (1998).
[37] M. Shehadeh, E. Bringa, H. Zbib, J. McNaney, and B. Remington, Applied Physics Letters **89**, 171818 (2006).
[38] J.C. Crowhurst, M.R. Armstrong, K.B. Knight, J.M. Zaug, and E.M. Behymer, Physical Review Letters **107**, 144302 (2011).
[39] R. Rohde, Acta Metallurgica **17**, 353 (1969).
[40] D. Grady, J. Appl. Phys. **107**, 013506 (2010).
[41] J. Gilman, *Micromechanics of Flow in Solids* (McGraw-Hill, 1969).
[42] R. Thomson, "Physics of fracture," (Academic Press, London, 1986) pp. 1–129.